Journal of Controlled Release 357 (2023) 287–298

Contents lists available at ScienceDirect

Journal of Controlled Release

journal homepage: www.elsevier.com/locate/jconrel

Radiosensitisation by olaparib through focused ultrasound delivery in a diffuse midline glioma model

E. 't Hart [a], J. Bianco [a], M.A.C. Bruin [b], M. Derieppe [a], H.C. Besse [c], K. Berkhout [a], L.A. Chin Joe Kie [a], Y. Su [a], E.W. Hoving [a], A.D.R. Huitema [a,b,d], M.G. Ries [c,1], D.G. van Vuurden [a,1,*]

[a] Princess Maxima Center for Pediatric Oncology, Heidelberglaan 25, 3584 CS Utrecht, the Netherlands
[b] Department of Pharmacy and Pharmacology, the Netherlands Cancer Institute, Antoni van Leeuwenhoek Hospital, Plesmanlaan 121, 1066CX Amsterdam, the Netherlands
[c] Center for Imaging Sciences, University Medical Center Utrecht, Heidelberglaan 100, 3584 CX Utrecht, the Netherlands
[d] Department of Clinical Pharmacy, University Medical Center Utrecht, Utrecht University, Heidelberglaan 100, 3584 CX Utrecht, the Netherlands

ARTICLE INFO

Keywords:
Diffuse midline glioma H3K27-altered
Radiosensitisation
PARP1
Blood-brain barrier
Focused ultrasound

ABSTRACT

Background and purpose: Diffuse midline glioma H3K27-altered (DMG) is an aggressive, inoperable, predominantly paediatric brain tumour. Treatment strategies are limited, resulting in a median survival of only 11 months. Currently, radiotherapy (RT), often combined with temozolomide, is considered the standard of care but remains palliative, highlighting the urgency for new therapies. Radiosensitisation by olaparib, an inhibitor of PARP1 and subsequently PAR-synthesis, is a promising treatment option. We assessed whether PARP1 inhibition enhances radiosensitivity *in vitro* and *in vivo* following focused ultrasound mediated blood-brain barrier opening (FUS-BBBO).

Methods: Effects of PARP1 inhibition were evaluated *in vitro* using viability, clonogenic, and neurosphere assays. *In vivo* olaparib extravasation and pharmacokinetic profiling following FUS-BBBO was measured by LC-MS/MS. Survival benefit of FUS-BBBO combined with olaparib and RT was assessed using a patient-derived xenograft (PDX) DMG mouse model.

Results: Treatment with olaparib in combination with radiation delayed tumour cell proliferation *in vitro* through the reduction of PAR. Prolonged exposure of low olaparib concentration was more efficient in delaying cell growth than short exposure of high concentration. FUS-BBBO increased olaparib bioavailability in the pons by 5.36-fold without observable adverse effects. A Cmax of 54.09 μM in blood and 1.39 μM in the pontine region was achieved following administration of 100 mg/kg olaparib. Although RT combined with FUS-BBBO mediated olaparib extravasation delayed local tumour growth, survival benefits were not observed in an *in vivo* DMG PDX model.

Conclusions: Olaparib effectively radiosensitises DMG cells *in vitro* and reduces primary tumour growth *in vivo* when combined with RT. Further studies are needed to investigate the therapeutic benefit of olaparib in suitable preclinical PDX models.

1. Introduction

Diffuse midline gliomas H3K27-altered (DMG) are WHO grade IV invasive, rapidly growing high-grade gliomas (HGG), occurring in the pons, thalamus, and spinal cord of children and young adults, and together with hemispheric HGG, account for 8–12% of all central nervous system tumours in children [1]. Despite years of intensive research, significant curative progress for pontine DMG, formally known as diffuse intrinsic pontine glioma (DIPG), has remained elusive [2]. As a consequence, the average survival of DMG patients is only 11 months, with a 95% fatality rate within 2 years of diagnosis [3,4]. Currently radiotherapy (RT), either as monotherapy or in combination with

* Corresponding author.
E-mail address: D.G.vanVuurden@prinsesmaximacentrum.nl (D.G. van Vuurden).
[1] Equal seniority

https://doi.org/10.1016/j.jconrel.2023.03.058
Received 2 December 2022; Received in revised form 21 March 2023; Accepted 31 March 2023
Available online 5 April 2023

temozolomide is the standard of care. Radical surgery is impossible due to the intrinsic nature and infiltrative growth of the tumour [5]. Although RT is not curative, 80% of the children display symptom relief and benefit from an increased life expectancy of 6 months [6,7]. Chemotherapy efficacy is generally hampered by a largely intact blood-brain barrier (BBB), lack of therapeutic targets and chemoresistance [8].

DMG/DIPG tumours display a compromised ability to repair double-strand DNA breaks (DSBs) due to the occurrence of P53 mutations and defective homologous recombination repair (HRR), possibly by amplification of cyclin D2 (CCND2) and TOP3A, and heterozygous mutations in HRR-related genes such as ATM, BRCA2, BLM, ATR, PALB2, RAD50 and RAD51C, and Fanconi anaemia related genes such as BRIP1, FANCM, FANCA, and FANCG [9,10]. DSB repair/HRR-deficient tumours are ideal candidates for poly(ADP-ribose) polymerase (PARP) inhibition therapy, as these tumours are more dependent on DNA single-strand break (SSB) repair, where PARP1 is an important player [11,12]. PARP1 is accountable for the detection and initiation of SSB repair through the synthesis of poly(ADP-ribose) (PAR) chains, which acts as a signal for other DNA-repair proteins [5,13,14]. If PAR-synthesis and subsequent DNA repair is impaired by PARP inhibition, SSBs are converted to DSBs that eventually lead to DSB repair by HRR, non-homologous end-joining or cell death in DSB repair deficient cells (synthetic lethality).

Pre-treatment with the PARP1 inhibitor olaparib, in combination with RT, has been shown to inhibit cell growth and DSB repair in several cell lines *in vitro*, including medulloblastoma, ependymoma, HGG, glioblastoma and DMG [15,16]. The potential radiosensitising effect has also been validated in *in vivo* models of lung, breast, glioblastoma, and pancreatic cancers [17–20]. Moreover, several clinical trials have been performed to validate this combined therapy effect [21–23]. To date, clinical trials involving PARP inhibition in combination with RT for primary brain tumours and metastases have not yet proven to be effective [24–27].

Delivery of radiosensitisers within the brain is complicated by the BBB, which prevents 98% of all small molecule and nearly 100% of the large molecules to cross and remain in the brain parenchyma [28–30]. To facilitate delivery of radiosensitisers across the BBB, focused ultrasound mediated blood-brain barrier opening (FUS-BBBO) has been suggested for local drug delivery. FUS-BBBO uses low frequency ultrasound waves to cause stable cavitation of intravenously injected microbubbles (MBs), resulting in BBB opening (BBBO) [31]. Mechanical interaction of MBs with the BBB temporarily cause the dislocation of tight junctions between endothelial cells and increased transcytosis, thereby enhancing permeability into the brain parenchyma [32,33]. Furthermore, BBB drug transporters are also thought to be affected by FUS-BBBO [34]. *In vivo,* FUS-BBBO has been shown to increase the concentration of molecules into the brain parenchyma by up to fifty-fold [35–37]. So far, FUS-BBBO with stable cavitation has displayed little to no side-effects and lasts for 4–24 hours (h), after which BBB function is restored [38,39].

The primary goal of this study was to investigate if FUS-BBBO enhances olaparib concentration in the brain, and when given in concert with RT inhibits tumour growth and prolongs survival of a xenograft DMG tumour model. In this study we therefore evaluated the radiosensitising effects of olaparib in two patient-derived DMG cell lines *in vitro*, as well as the extravasation of olaparib into the pons by FUS-BBBO *in vivo*. *In vivo*-like pharmacokinetic (pK) profiles were applied to DMG neurosphere cultures *in vitro* to assess radiosensitisation before potential benefit of this combination therapy was validated in a patient-derived xenograft (PDX) tumour model.

2. Materials and methods

2.1. Cell lines and culture

HSJD-DIPG-007 and HSJD-DIPG-011 DIPG cells were obtained from the University of Barcelona and were grown as suspension cultures in 1:1 Neurobasal-A and Advanced DMEM/F-12 medium containing working concentrations of 10 mM HEPES buffer, 1 × MEM non-essential amino acids, 1% GlutaMAX, 1 mM Sodium pyruvate, 1 × B-27 minus vitamin-A, 10 ng/ml PDGF-AA, 10 ng/ml PDGF-BB (all from ThermoFisher, USA), 20 ng/ml bFGF, 20 ng/ml EGF (Princess Maxima Center pharmacy), 2 μg/ml heparin (StemCell Technologies, Germany) and 1 mg/ml primocin (InvivoGen, USA). KNS42 glioma cells were obtained from Xenotech (IFO50356) and were grown as adherent cultures in DMEM/F-12 supplemented with 10% heat-inactivated foetal bovine serum (FBS, ThermoFisher) and 100 μg/ml penicillin/streptomycin (ThermoFisher). Cell lines were maintained at a constant temperature of 37 °C and 5% CO_2 and a humidity of 95%, with media changes every 3–4 days. For *in vivo* PDX mouse models, HSJD-DIPG-007 cells were chosen for grafting into male hosts as they are a well characterised cell line derived from the brainstem/pons of a male paediatric patient (Accession: CVCL_VU70), whereas HSJD-DIPG-011 cells are derived from a female paediatric patient [40]. HSJD-DIPG-007 cells were transduced to express firefly luciferase following a previously described protocol [41], enabling *in vivo* tumour growth monitoring through bioluminescence imaging (BLI). Briefly, HEK293T cells were transfected with Polyethylenimine (PEI) using an envelope plasmid (pHDMG (ENV)), packing plasmids (pHDMG-Hgpm2, pRC/CMV-Rev1b, pHDM-Tat1b) and a transfer plasmid (eGFP-ffLuc_epHIV7) for lentiviral plasmid production. HSJD-DIPG-007 cells were then infected, and eGFP-lucF-gene positive cells were sorted using a Sony SH800 Cell Sorter (Sony, Japan).

2.2. Animals

For pharmacokinetic profiling and safety of the FUS-BBBO/olaparib combination, 6–12-week-old naïve female athymic nude Foxn1−/− mice (n = 25, Charles River, France) were used. For PDX survival studies, 5–6-week-old male athymic nude Foxn1−/− mice (n = 42, Envigo, France) were used. Mice were housed under pathogen-free conditions in individually ventilated cages in groups up to five and maintained on standard laboratory food and water *ad libitum*, with a fixed 12-h light/dark cycle in compliance with ARRIVE guidelines [42]. For the purposes of this study, gender dimension was considered to be partly relevant. Although a recent study assessing the effects of mouse gender on tumorigenicity, xenograft growth and drug response in a large panel of PDX models of paediatric brain tumours demonstrated that mouse gender did not significantly impact measurable outcomes [43], recent studies have shown that olaparib pharmacokinetics in rats is gender-dependent, with low clearance, long half-life, high plasma exposure and high viability seen in female rats compared to males. As our study wanted to show that olaparib extravasation can be achieved with FUS-BBBO, female animals were selected for the pharmacokinetic profiling phase [44,45]. For PDX studies, male hosts were used in order to sex-match donor cells, which were derived from the brainstem/pons of a male paediatric patient [40].

2.3. Drugs and contrast agents

For *in vitro* experiments, a 10 mM stock solution of olaparib (434.46 Da, AZD-2281, MedChemExpress, Sweden) was prepared in dymethylsulfoxide (DMSO). For *in vivo* studies, olaparib was prepared with 3% DMSO and 10% (2-Hydroxypropyl)-β-cyclodextrin in phosphate buffered saline (PBS) at 5 mg/ml before i.p. injection. Pre- and post-surgical pain was managed with carprofen p.o. (67 μg/ml in drinking water, Faculty of Veterinary Medicine pharmacy, Utrecht, Netherlands) and s.c. injection (5 mg/kg), lidocaine (s.c., 0.5%, B. Braun, Germany) and buprenorphine hydrochloride (s.c., 0.05 mg/kg, Temgesic, Schering-Plough, Netherlands). Surgical anaesthesia was with Isoflurane mixed with air (3% for induction, 1.8% for maintenance, 2 l/min O_2). Anaesthesia for irradiation was induced with dexmedetomidine (s.

c., 50 μg/kg in 0.9% saline, Orion Pharma, UK) and reversed with atipamezole hydrochloride (s.c., 13.3 mg/kg, Alzane, Laboratorios Syva, Spain). D-luciferin Potassium Salt (i.p., 150 mg/kg, in PBS, Cayman Chemical, Netherlands) was used for monitoring engrafted cells. Blood coagulation was prevented with heparin (50 UI/kg, Leo Pharmaceuticals, Netherlands). A 4% *v*/v Evans blue solution (filtered, in PBS, Sigma Aldrich, Netherlands) was used to assess BBB integrity. Euthanasia was performed using 10:1 Ketamine:Sedazine (7.14 mg/ml and 0.714 mg/ml respectively, in PBS, Alfasan and AST Farma, Netherlands).

2.4. Cell viability

For viability analysis, HSJD-DIPG-007 and -011 cells were seeded in triplicate in black, clear bottom 96 well culture plates (Corning, USA) at a density of 2500 cells/well in normal culture conditions as described above. Cultures underwent a 30 minutes (min) exposure of vehicle or olaparib (0.01–3 μM concentration range) before irradiation with 0–4 Gy using a benchtop cell irradiator (1.66 Gy/min, 130 kV, 5.0 mA, Cellrad, Precision, USA), after which they were maintained with constant drug exposure for 72 h, in accordance with previous studies that have established 72 h as optimal screening duration for *in vitro* oncolytic compounds in 3-dimensional cultures [46,47]. Cell viability was then determined using the CellTiter-Glo® 3D Cell Viability Assay (Promega, USA) according to the manufacturers' instructions, and the resulting luminescence signal was measured using a Spectramax iD3 plate reader (Molecular Devices, USA).

2.5. Clonogenic survival

To assess clonogenic survival, the soft agar method was used as previously described [4]. Briefly, a 0.33% agar suspension containing HSJD-DIPG-007 and -011 single cells was plated over a 0.5% agar underlay in 24 well plates, at a density of 800–6400 cells/well. Cells were pre-treated with vehicle or olaparib (0.1–1 μM) 30 min before irradiation (0–2 Gy) as described above. Cultures were maintained for 10–14 days with constant drug exposure under normal culture conditions after which colony growth was assessed using a Thiazolyl Blue Tetrazolium Blue (MTT) assay (Sigma-Aldrich). Surviving fractions were calculated based on the colonies times the plating efficacy. The plating efficacy was calculated by colonies divided by cell seeding as previously described [48].

2.6. Neurosphere growth

For neurosphere growth assays, HSJD-DIPG-007 and -011 were plated as single cells in low attachment, U-bottom 96 well culture plates (400 cells/well, BRANDplates®, Sigma-Aldrich) and neurospheres were allowed to form for 4 days before being exposed short-term (2 h) to either 0.68 or 1.36 μM olaparib, or long-term (72 h) to either 0.018 or 0.036 μM olaparib, after which they were transferred to drug-free medium. At 30 min after initial exposure to olaparib, neurospheres received 1.8 Gy radiation fractions/day for 5 consecutive days (9 Gy total). Non-irradiated exposed cells served as control, and cultures were maintained up to 28 days. Growth was monitored with a Leica DMi1 microscope (Leica Biosystems, Netherlands) and size was quantified by ImageJ [49].

2.7. Western blot

For western blot analysis of PARP1, PAR and β-actin protein expression, cells were plated in normal culture conditions as described above as single cells and allowed to acclimatise for 24 h, after which a 6 h treatment with olaparib ranging from 1 to 5 μM, with or without 1.8 Gy radiation was performed. Non-treated, irradiated cells were used as controls. Following treatment, HSJD-DIPG-007 and -011 cells were collected, pelleted, and lysed with ice cold RIPA lysis buffer (ThermoFisher) containing Halt protease and phosphatase inhibitors (1:100, Bio-Rad, USA). For adherent KNS42 cultures, cells were washed twice with PBS before ice cold RIPA buffer was directly added to the culture flasks, after which the cells were dislodged using a cell scraper. Cell suspensions were then transferred to pre-cooled microcentrifuge tubes and centrifuged at 4 °C for 30 min at maximum speed. The protein containing supernatant was transferred to a new tube and kept on ice. Protein concentrations were determined using a Pierce BCA Protein Assay Kit (ThermoFisher) as per manufacturers' instructions. Lysates of equal protein concentrations were separated using 10% SDS-PAGE, followed by electrotransfer to PVDF membranes using the Trans-Blot® Turbo™ transfer system (all from Bio-Rad). The membranes were then blocked with 5% non-fat dry milk (in 20 mM Tris, 137 mM NaCl, 0.1% Tween) for 1 h at room temperature before incubation overnight at 4 °C with either rabbit anti-PARP1 antibody (1:500, #9542, Cell Signaling Technology, USA), rabbit anti-PAR antibody (1:500, #4336-BPC-100, Trevigen, USA), or mouse anti-β-actin antibody (1:5000, #A5441, Sigma-Aldrich). Membranes were then washed and incubated with an appropriate swine anti-rabbit or rabbit anti-mouse horseradish peroxidase (HRP) conjugated secondary antibody (1:500, #P021702–2 or #P016102–2, IgG, Agilent Dako, USA) for 1 h at room temperature. Protein bands were detected using enhanced chemiluminescence (Bio-Rad) and expression was quantified using ImageJ [49].

2.8. BBBO by FUS and olaparib pK values

The procedure for image-guided MB mediated FUS-BBBO using an in-house stereotactic platform has been previously described in detail [50]. To manage acute perioperative pain, mice ($n = 25$) were administered with 0.05 mg/kg buprenorphine *via* i.p. injection 15 min before anaesthesia with isoflurane. Once sedated, a 26-gauge catheter (Neoflon, Bectom Dickinson, Sweden) was placed in the lateral tail vein and flushed with heparin to prevent blood coagulation. Mice were then mounted on a custom-made platform and secured in place with ear bars. X-ray imaging for transducer guiding/targeting was performed with the *In-Vivo* Xtreme™ optical imaging system (Bruker, Germany). Mice were then placed onto the stereotactic platform and a hydrophone (Precision Acoustics, United Kingdom) was positioned behind the left ear of the animal to monitor scattered cavitation signal. A connection with an ultrasonic mono-element focused transducer was made with ultrasound gel. MBs (60 μl, SonoVue, Bracco, Amsterdam) [51] were administered through the tail vein catheter, and FUS was initiated at 1 MHz, with 1.6 Hz pulse repetition frequency (PRF) and 400 kPa pressure, in a hexagonal pattern of 10 millisecond tone bursts, with a second boli of MBs administered at 60 seconds (s) from the start of FUS-BBBO (total duration of 120 s).

Depending on group, mice underwent FUS-BBBO exposure as described above before receiving either 10 or 100 mg/kg olaparib immediately following the procedure *via* i.p. in 4 sub-injections at 5 min intervals. Mice were then sacrificed after 15, 30, 45 and 120 min after drug administration. Before sacrifice, Evans blue was injected i.p. to assess BBB permeability. Mice were then deeply sedated with ketamine/sedazine after which blood was collected *via* cardiac puncture after which animals were transcardially perfused with 50 ml saline. Brain tissue, organs, muscle, and blood/plasma were collected and stored at −80 °C for histological or liquid chromatography–mass spectrometry (LC-MS/MS) analysis. The experimental design is outlined in Fig. 1 A.

2.9. Survival analysis upon RT and olaparib extravasation in a PDX model

Inoculation of HSJD-DIPG-007 xenografts have been previously described [52]. In brief, 24 h before and after intracranial injection, mice received 0.067 mg/ml carprofen p.o. in drinking water. 30 min pre-surgery, mice also received a s.c. injection of 5 mg/kg carprofen for acute perioperative pain management. Mice were then anaesthetised with isoflurane and fixed in a stereotactic frame. Once immobile, a 5 mm

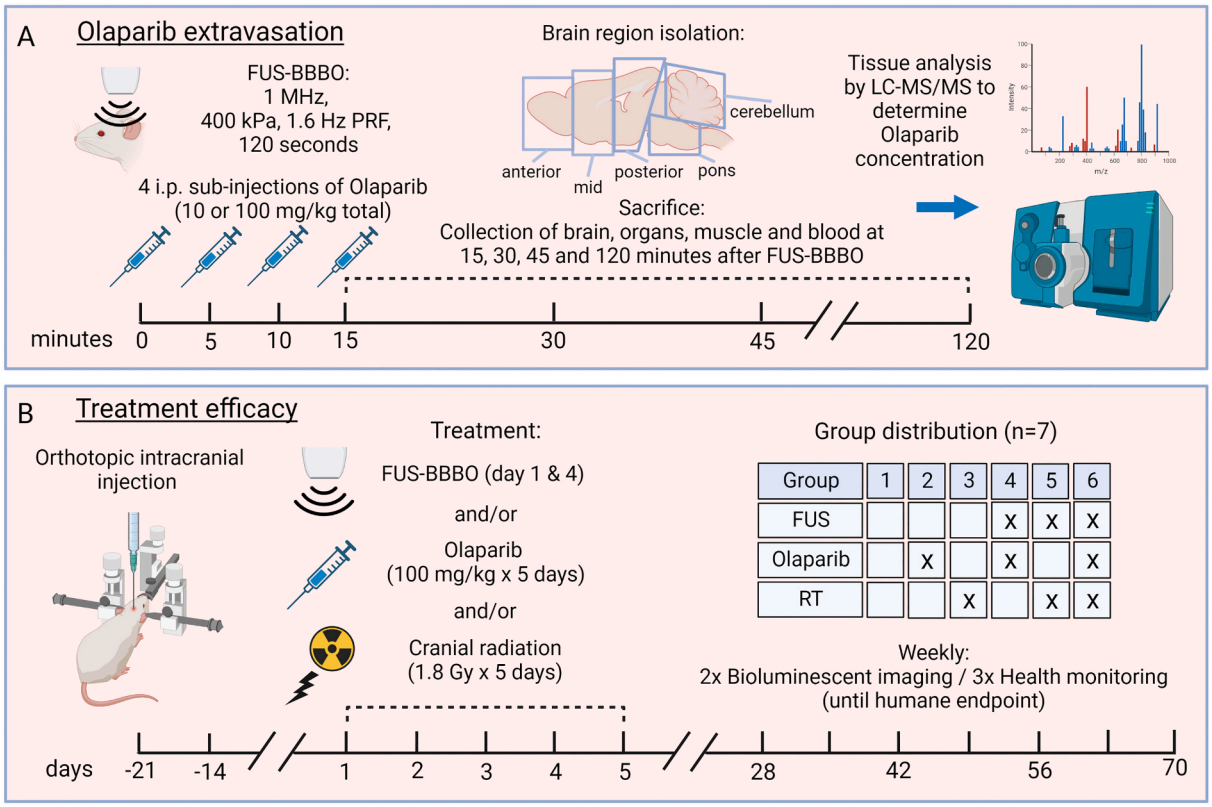

Fig. 1. Experimental design of olaparib extravasation *via* FUS-BBBO and subsequent assessment of treatment efficacy in combination with radiotherapy. (A) Outline of pharmacokinetic profiling of olaparib following FUS-BBBO. A total of 10 or 100 mg/kg olaparib was administered within 15 min following FUS-BBBO, after which tissue samples (brain, organs, muscle, blood) were collected at 15-, 30-, 45-, and 120-min post administration to determine olaparib concentration by LC-MS/MS analysis. (B) Outline of treatment efficacy to determine radiosensitising effects of olaparib in combination with radiotherapy and FUS-BBBO in a DMG PDX mouse model using 100 mg/kg olaparib per day for 5 days. Tumour growth was monitored with bioluminescent imaging until humane endpoints were reached.

long incision was made along the midline, after which a burr hole was drilled into the skull 0.8 mm posterior and 1.0 mm lateral to the lambda using a high-speed drill. A 5 μl Hamilton syringe fitted with a 26-gauge needle was then used to inject 5 μl of PBS containing 5×10^5 eGFP-lucF-HSJD-DIPG-007 cells at a depth of 4.5 mm, at a rate of 2 μl/min. After injection, the needle was kept in place for 7 min before being slowly extracted as a measure to prevent cells accumulating into the needle track. The wound was closed using topical skin adhesive (Histoacryl, B. Brand, Germany), and the animals were transferred under a heating lamp and allowed to awaken, while signs of distress and post-operative complications were closely monitored. Mouse weight was monitored 3 times/week, while tumour grafting was confirmed, and progression monitored, through BLI twice a week until humane euthanasia endpoints were reached. The human euthanasia endpoints were determined based on 20% weight loss from the beginning of the treatment, 15% weight loss in two days or showing symptoms related to neurological deficiencies. One animal in group 2 died prematurely before treatment, and one animal in group 6 died during FUS-BBBO procedure. Mice were anaesthetised with isoflurane and injected (i.p.) with 150 mg/kg D-luciferin before BLI signal detection using the MILABS U-OI system (MILABS, Netherlands). Three BLI scans were performed at 5, 10 and 15 min after D-luciferin injection (60 s exposure time). BLI data was analysed using customized software in MATLAB (MATLAB version R2020a) to determine BLI signal intensity by verification of the highest signal measured. After death/sacrifice, brains were extracted and fixed in 10% formalin (Sigma-Aldrich) for histological analysis.

Based on BLI signal, at 21 days after intracranial implantation, mice were evenly distributed in 6 groups ($n = 7$): 1) control, 2) olaparib, 3) RT, 4) FUS-BBBO+olaparib, 5) FUS + RT, 6) FUS-BBBO+olaparib+RT. Group 1 (control) received 0.9% saline i.p. injections for 5 consecutive days. Groups 2, 4, 5, and 6 underwent MB mediated FUS treatment on days 1 and 4. Groups 3, 5, and 6 underwent daily cranial radiation of 1.8 Gy in a small-animal irradiator (whole head, 200 kV, 4.0 mA, Yxlon International AS, Denmark) for 5 consecutive days, following identically adjusted conditions used for *in vitro* radiation analyses. Groups 2, 4, and 6 received 100 mg/kg olaparib *via* i.p. injection for 5 consecutive days. When treatments were combined, olaparib was given immediately after FUS with 4 sub-injections at 5 min intervals (at time 0, 5, 10 and 15 min). Thirty minutes after FUS and/or 15 min after the last sub-injection of olaparib, RT was given. The experimental design is outlined in Fig. 1 B.

2.10. Liquid chromatography–mass spectrometry (LC-MS/MS)

Collected blood was centrifuged at 1500 *g* for 15 min at 4 °C, and the resulting plasma phase was stored at −20 °C until analysed. Following exsanguination, whole brain, heart, lung, liver, kidney, spleen and left hindleg muscle were rapidly removed, weighed, and stored at −80 °C until processed. Before analysis, tissues were homogenized in an appropriate volume of control human lithium heparin plasma (Bioreclamations LLC, USA) using a FastPrep-24™ 5G Grinder (MP Biomedicals, USA) and stored at −20 °C until analysed.

Olaparib concentrations in plasma and tissue homogenates were analysed using a previously reported and validated liquid-chromatography mass spectrometry (LC-MS/MS) method [53]. Validation of the assay on mouse tissue was performed by spiking brain homogenate with olaparib at a final concentration of 400 ng/ml before analysis on a human lithium heparin plasma calibration curve. The intra-run accuracy and precision were − 6.8% and 5.2% respectively, and within the required ±15% according to FDA and EMA guidelines

[54,55]. For quantification, 10 μl mouse plasma was added to 90 μl lithium heparin plasma. The limit of detection was set to 0.3 ng/ml (limit of quantification range 1 ng/ml – 5000 ng/ml). Total concentration measured by LC-MS/MS are free and protein-bound fractions of olaparib.

2.11. Histological analysis

To determine histopathological elements, tumour size, location and proliferation, haematoxylin and eosin (H&E) and human vimentin staining was performed as previously described [56]. Following

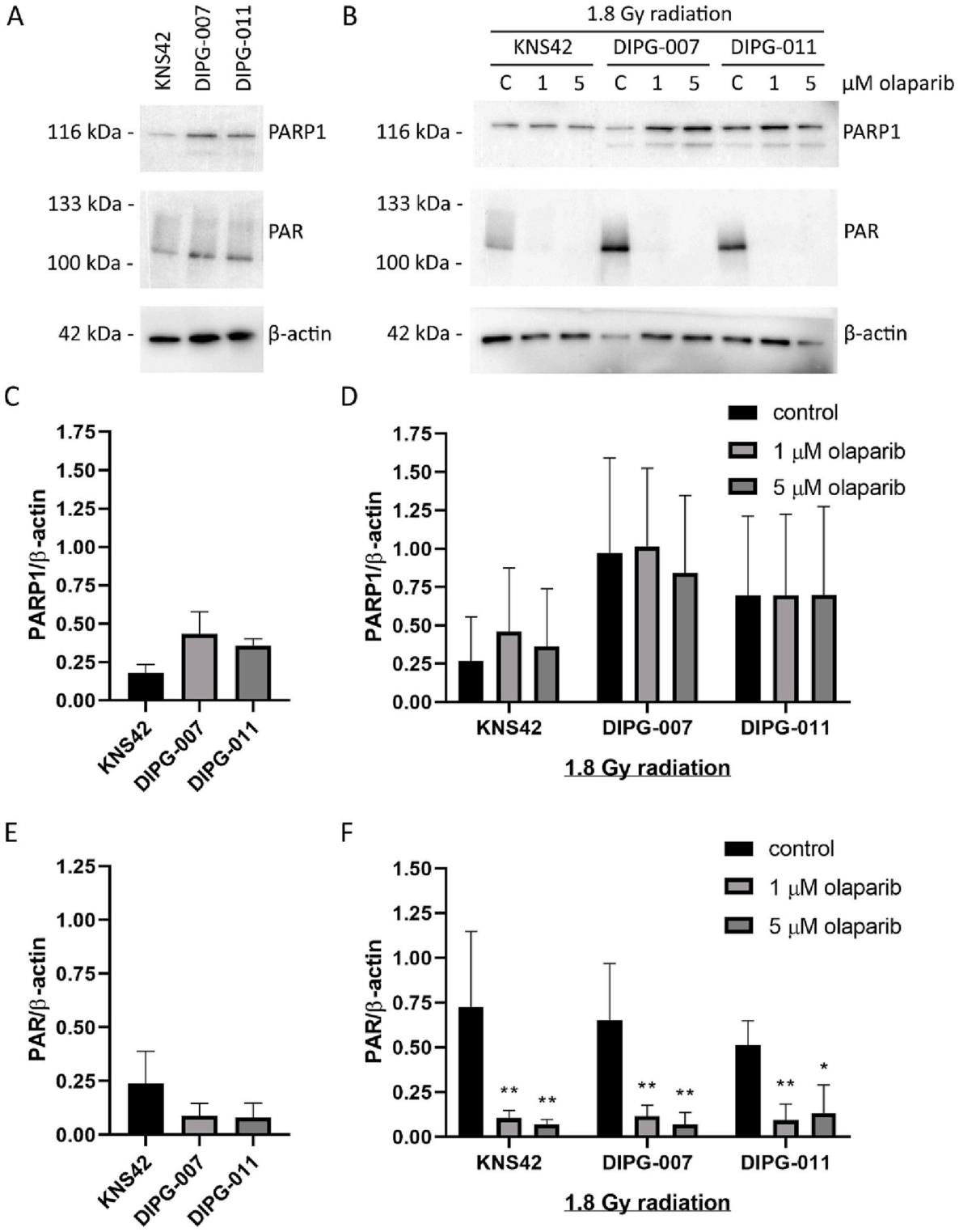

Fig. 2. PARP1 and PAR expression in glioma and DIPG cell lines. Western blot analysis of KNS42, HSJD-DIPG-007 and HSJD-DIPG-011 cell lines showing intrinsic expression levels of PARP1 and PAR in untreated, non-irradiated cells (A) and after 6 h treatment with or without 1 or 5 μM olaparib and 1.8 Gy radiation, showing inhibition of PAR-synthesis upon treatment with olaparib (B). Densitometry data of WB analysis showing PARP1 levels in untreated cells (C) and following olaparib/radiation treatment (D). Densitometry data of WB analysis showing PAR levels in untreated cells (E) and following olaparib/radiation treatment (F). Data points are expressed as mean ± SD ($n = 3$), *$p < 0.05$, **$p < 0.01$.

euthanasia and perfusion, brains were excised and fixed in 10% formalin before embedding in paraffin, after which 4 μm sagittal sections were made using a microtome (Leica Biosystems) and mounted onto glass cover slides. Sections were deparaffinised before use and underwent antigen retrieval in sodium citrate buffer (10 mM, 95–100 °C, 30 min) before staining for human vimentin. Endogenous peroxidase activity was quenched by immersing the slides in 3% hydrogen peroxide (in PBS) for 20 min, followed by two rinses in deionised water and one rinse in PBS-Tween. Sections were then blocked using antibody diluent clear (VWRKBD09–125, VWR, USA) for 1 h at room temperature before incubation with rabbit anti-human vimentin [SP20] (1:5, ab27608, Abcam, England) overnight at 4 °C. Sections were then washed and incubated with a biotinylated affinity-purified goat anti-rabbit secondary antibody (1:500, BA-1000, IgG (H + L), Vector Laboratories, USA) for 2 h at room temperature. Following secondary antibody incubation, VECTASTAIN® Elite ABC-HRP Peroxidase (PK-6100, Vector Laboratories) was applied for 2 h, followed by a 3 min incubation in 3,3′-diaminobenzidine (DAB, K346711–2, Agilent Dako). Sections were then counterstained with haematoxylin, dehydrated in a graded series of alcohol, immersed in xylene, and mounted using Permount™ mounting medium (ThermoFisher).

2.12. Data processing and statistical analysis

Western blots, cell viability and clonogenic assays were statistically verified using a two-way ANOVA. Extravasation of olaparib was analysed using the Mann-Whitney *U* test. Survival was analysed using a Kaplan-Meier and Log-rank test. A *p*-value of ≤ 0.05 was considered statistically significant. The statistical analyses were performed using GraphPad Prism (version 9, GraphPad Software, LLC, USA).

3. Results

3.1. In vitro radiosensitisation of DMG cells by PARP1 inhibition

Western blot showed that HSJD-DIPG-007 and -011 (DMG) cells display higher PARP1, but lower PAR activity than KNS42 (glioma) cells (Fig. 2 A, C, E), which was further increased following 1.8 Gy radiation (Fig. 2 B, D, F). Radiation alone elevated PARP1 expression by 2.34- and 1.95-fold in HSJD-DIPG-007 and -011, respectively, and 2.55-fold in KNS42, and was not affected by the addition of olaparib (Fig. 2 C, D). Radiation alone elevated PAR expression by 7.42- and 6.42-fold the DMG and 3.04-fold in glioma cells but was significantly inhibited when combined with olaparib in all three cells lines (Fig. 2 E, F).

Cell exposure to olaparib as a single treatment modality showed that

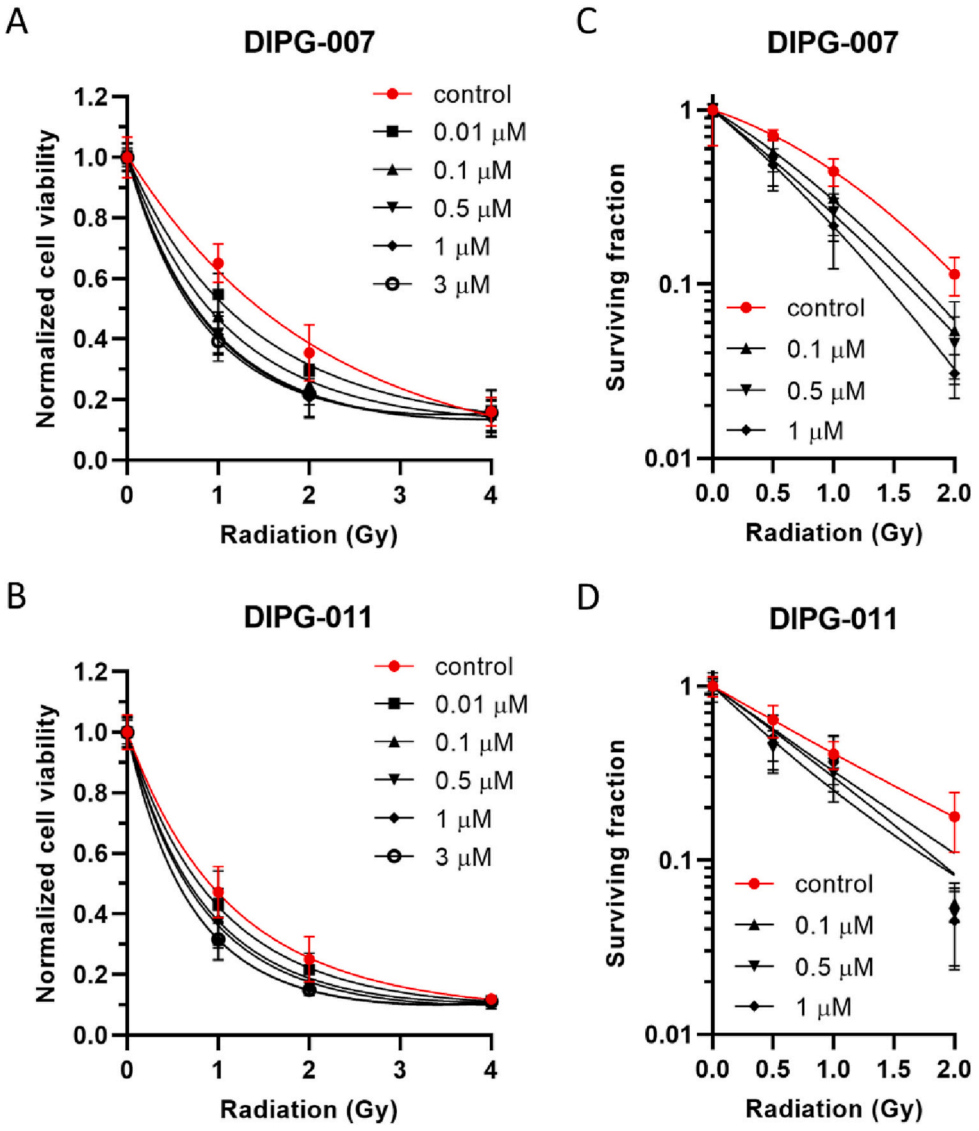

Fig. 3. Cell viability and clonogenic survival of DIPG cell lines. Viability of HSJD-DIPG-007 (A) and HSJD-DIPG-011 (B) cells 72 h following 0–4 Gy radiation alone or in combination with a 30 min pre-treatment of 0.01–3 μM olaparib, showing a viability reduction in both cell lines. Significant differences were found in all treatment groups (except 0.01 μM) at 1.0 and 2.0 Gy ($p < 0.05$). Clonogenic capacities were reduced in HSJD-DIPG-007 (C) and HSJD-DIPG-011 (D) cells 10–14 days after 0–2 Gy radiation alone or in combination with a 30 min pre-treatment of 0.1–1 μM olaparib. Significant differences were found at all treatments (except 0.1 μM) in at 0.5 and 1.0 Gy in HSJD-DIPG-007, and only at 0.5 Gy in HSJD-DIPG-011 ($p < 0.05$). Normalised data points are expressed as mean ± SD ($n = 3$).

HSJD-DIPG-007 and -011 have similar cell viability sensitivity to olaparib with a 50% inhibitory concentration (IC_{50}) of 3.4 and 4.1 μM respectively (data not shown). Pre-treatment 30 min before 1.8 Gy radiation demonstrated radiosensitising effects of olaparib through a decrease in cell viability compared to control cells, where HSJD-DIPG-007 was more sensitive to the combination treatment, while HSJD-DIPG-011 was more affected by radiation alone (Fig. 3 A, B). Clonogenic capacities were also reduced with the combination treatment in both DIPG cell lines (Fig. 3 C, D).

3.2. FUS-BBBO and local olaparib extravasation in the pons

Based on radiosensitisation properties of olaparib *in vitro*, extravasation of 10 mg/kg olaparib after FUS-BBBO was investigated. Stable cavitation in the vicinity of the pons was monitored *via* passive cavitation detection (fig. S1), with effective BBBO observed through extravasation of Evans blue (Fig. 4 A). A significant increase of olaparib was observed in the pons (5.36-fold) and cerebellum (3.18-fold) 30 min after injection combined with FUS-BBBO, while no elevation was observed in the posterior, middle and anterior cerebrum based on the blood/tissue ratio at that time point (Fig. 4 B). Based on total concentration, a significant difference in the pons and cerebellum after FUS-BBBO was observed, with no apparent increase in other brain regions or tissues examined (fig. S2 A, B). Pharmacokinetic profiling of olaparib in blood, following administration of 10 mg/kg i.p., showed a Cmax of 1978 ± 446.75 ng/g (4.55 μM), a Tmax of 30 min, an area under the curve (AUC) of 1833.11 $ng.g^{-1}.h$ (4.22 μM.h), and a $T_{1/2}$ of 15.05 min. Pharmacokinetic profiling of olaparib in the pons with FUS-BBBO showed a Cmax of 149.38 ± 84.19 ng/g (0.34 μM) tissue, a Tmax of 30 min, an AUC of 151.64 $ng.g^{-1}.h$ (0.35 μM.h), and a $T_{1/2}$ of 15.34 min (Fig. 4 C, D). When 100 mg/kg of olaparib was administered in combination with FUS-BBBO, compared to 10 mg/kg, an 11.88-fold (54.09 μM) increase in blood concentration was observed, with only a 4.04-fold increase in the pons (Cmax of 603.2 ± 179.68 ng/g tissue, equating to 1.39 μM) (Fig. 4 E, F). Dose-related neurotoxicity of 100 mg/kg olaparib in combination with FUS-BBBO was not observed within 24 h of administration (data not shown).

3.3. Pharmacokinetics parameters upon FUS-BBBO decreases in vitro neurosphere growth

The pK profiles of olaparib extravasation with FUS-BBBO were used to mimic conditions *in vitro* using a neurosphere growth assay. Based on pK profiling (100 mg/kg), a potential *in vivo*-tissue AUC of 1.41 μM.h olaparib (4.04-fold increase of 10 mg/kg AUC) was predicted. To test olaparib potency, AUCs of 1.3 and 2.6 μM.h were investigated at short (2 h) or prolonged (72 h) exposure times in combination with RT. Treatment with 9 Gy (5 × 1.8 Gy) radiation alone delayed HSJD-DIPG-007 and -011 neurosphere growth by 14–18 days (Fig. 5 A, B). While no differences were observed in HSJD-DIPG-007, radiation with prolonged

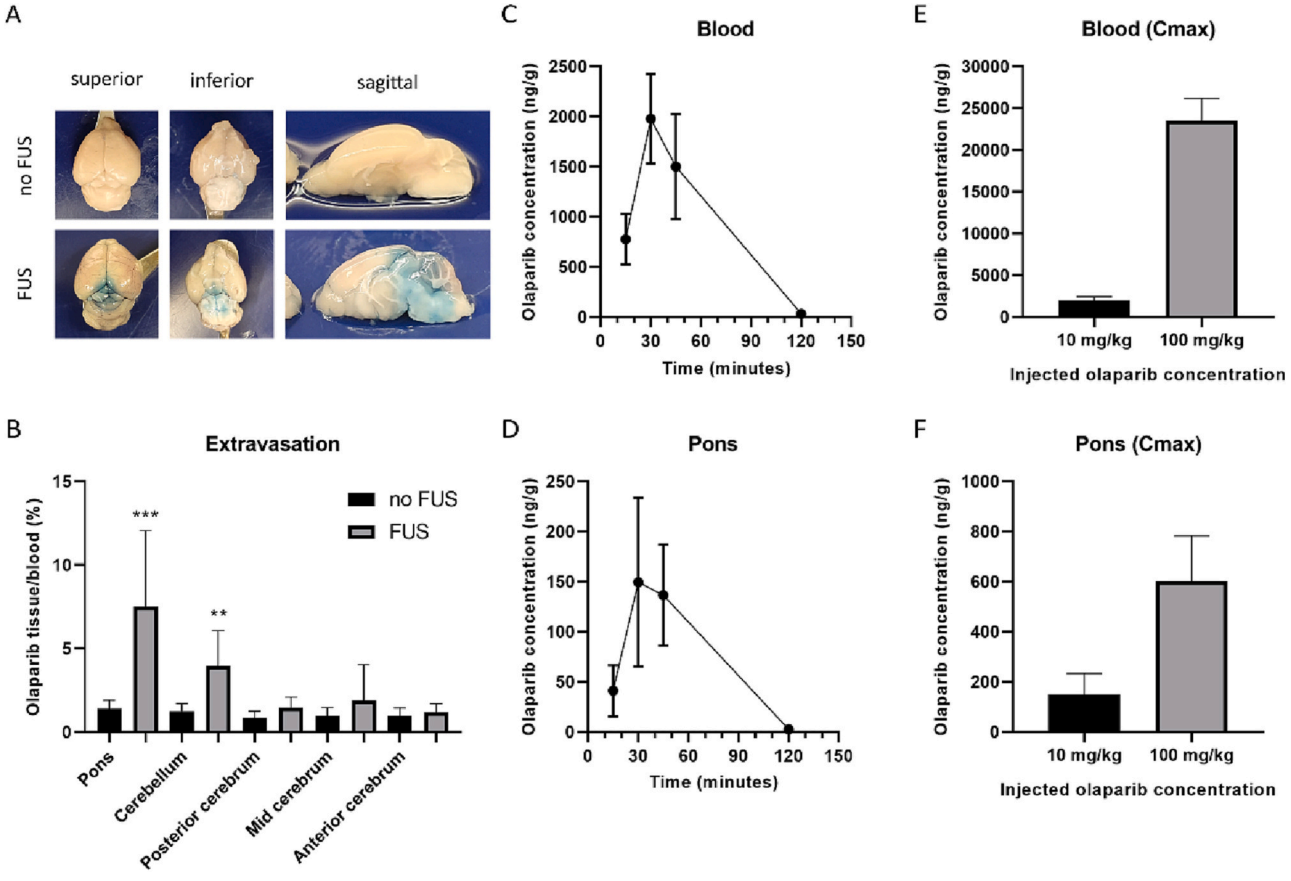

Fig. 4. FUS-BBBO, local extravasation of olaparib and pK value determination. (A) Evans blue extravasation with or without FUS-BBBO in the pontine region. (B) Blood/tissue ratios of olaparib administered alone or 30 min after FUS-BBBO showed a significant increase in the pons (5.36-fold) and cerebellum (3.18-fold), while no significant elevations were observed in the posterior, middle and anterior cerebrum. Measurements at 15-, 30-, 45-, and 120 min post olaparib administration (10 mg/kg) following FUS-BBBO revealed a Cmax of 1978.75 ± 446.75 ng/g (4.55 μM) olaparib in blood (C) and 149.38 ± 84.19 ng/g in the pons (0.34 μM) (D), and a Tmax of 30 min was found in both blood and pons. Following FUS-BBBO and administration of 10 mg/kg or 100 mg/kg of olaparib, an 11.88-fold increase (23,500 ng/g ± 2687, 54.09 μM) in Cmax was observed in blood (E), while a 4.04-fold increase (603 ng/g ± 179.68, 1.39 μM) in Cmax was observed in the pons (F). Data points are expressed as mean ± SD. $^{**}p < 0.01$, $^{***}p < 0.001$. (For interpretation of the references to colour in this figure legend, the reader is referred to the web version of this article.)

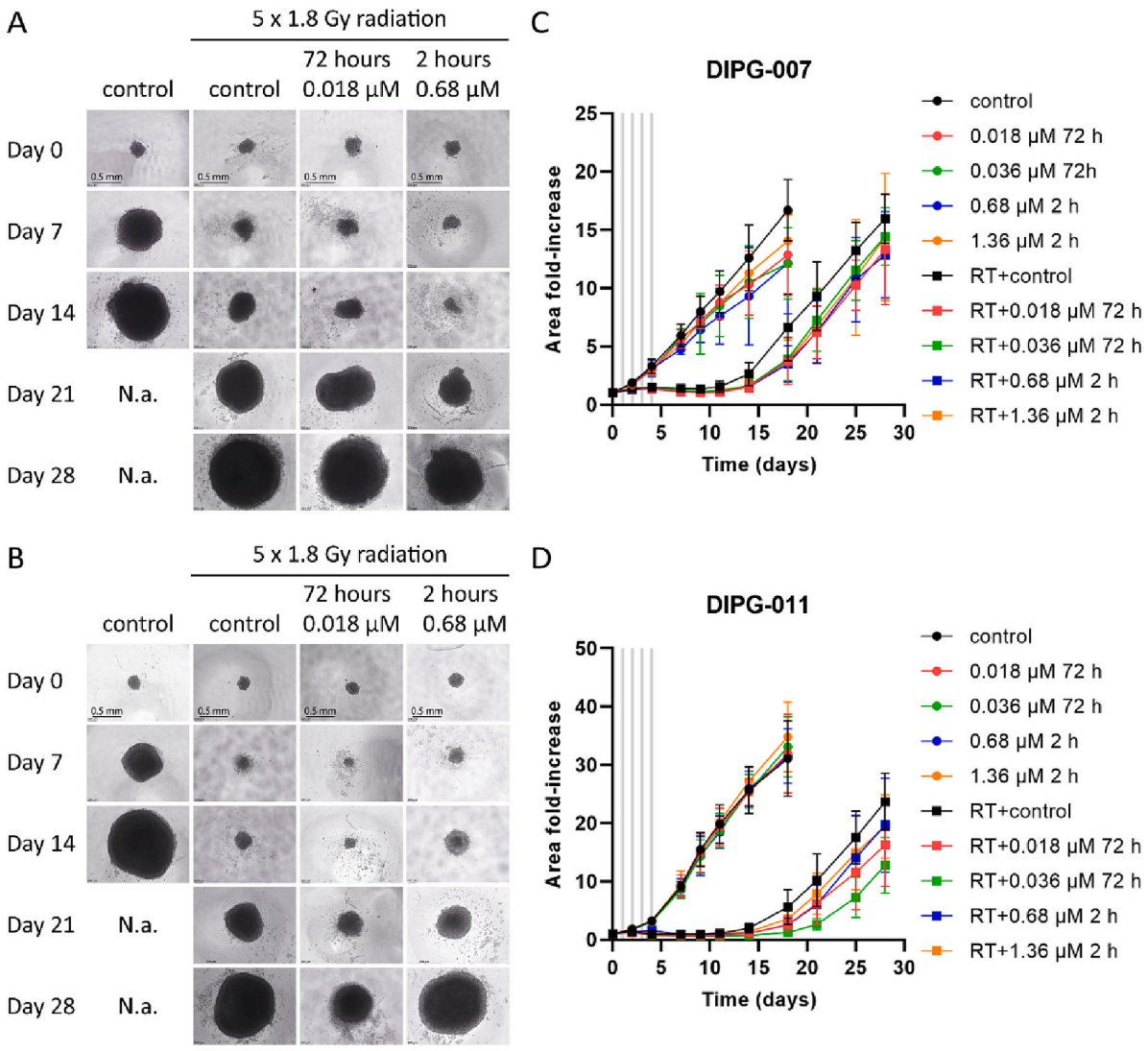

Fig. 5. Neurosphere radiosensitisation based on *in vivo* pK values. Daily dose of 1.8 Gy fractionated radiation (9 Gy total) delayed neurosphere growth by 14 days in both HSJD-DIPG-07 (A) and HSJD-DIPG-011 (B). Both short (2 h) and prolonged exposure (72 h) of varying olaparib concentrations extended regrowth delay in HSJD-DIPG-007 (C) and HSJD-DIPG-011 (D) in a dose/time dependant manner. Neurosphere growth was monitored until 18- or 28-days post radiation/olaparib treatment until spheres outgrew the imaging field and were too large to assess. Significant differences were found in all treatment groups with RT and olaparib compared to RT alone after 18 days of treatment for HSJD-DIPG-007 (except for 0.036 µM on day 21, 25 and 28 and 1.36 µM on day 28) and HSJD-DIPG-011 (except for 0.018 µM on day 18, 0.68 µM on day 18, and 1.36 µM on day 18, 21 and 25) ($p < 0.05$).

exposure to low olaparib concentrations delayed neurosphere regrowth more efficiently than short exposure to high concentration in HSJD-DIPG-011, despite a comparable AUC (Fig. 5 C, D).

3.4. Treatment efficacy upon FUS-BBBO olaparib extravasation and RT in a PDX model

Next, efficacy of olaparib and radiation was assessed *in vivo* using a HSJD-DIPG-007 PDX mouse model, 21 days post intracranial injection. Although no survival benefit was observed between groups (Fig. 6 A), local BLI signal in the pons did indicate tumour growth delay in animals treated with RT, irrespective of any other treatment paradigm (Fig. 6 B, C). Vimentin staining showed observable differences between groups. Metastatic formations were present in the olfactory bulbs of 45% of all animals, while primary pontine tumour growth was delayed in RT, and interestingly more so in fully (FUS-BBBO/olaparib/RT) treated animals (Fig. 6 D). No visible histological differences between groups were observed in olfactory bulbs and pons, based on H&E staining (fig. S3).

4. Discussion

DMG remains one of the most lethal paediatric tumours, with no curative efficacy of current treatment options. Previous studies have shown that PARP inhibition, in combination with radiation, is efficacious both *in vitro* and *in vivo* [57], and that FUS-BBBO can effectively disrupt the BBB to facilitate drug delivery [58]. This study's main goal was to investigate if enhanced delivery of PARP inhibitors *via* FUS-BBBO can, when combined with RT, improve therapeutic response in a DMG PDX model. We investigated the hypotheses that (I) elevated PARP expression in DMG cells represents potential therapeutic targets, (II) FUS-BBBO qualitatively improves the transport of olaparib across the BBB into the brain parenchyma, (III) *in vivo* realistic pK values in combination with RT can be mimicked *in vitro* with a potential therapeutic benefit, and (IV) olaparib extravasation by FUS-BBBO is potentially beneficial in xenograft model when combined with RT.

Our *in vitro* findings in DMG cell lines confirm previously reported elevated levels of PARP expression [12,15,16], and showed that inhibition of PAR-synthesis by olaparib significantly enhances

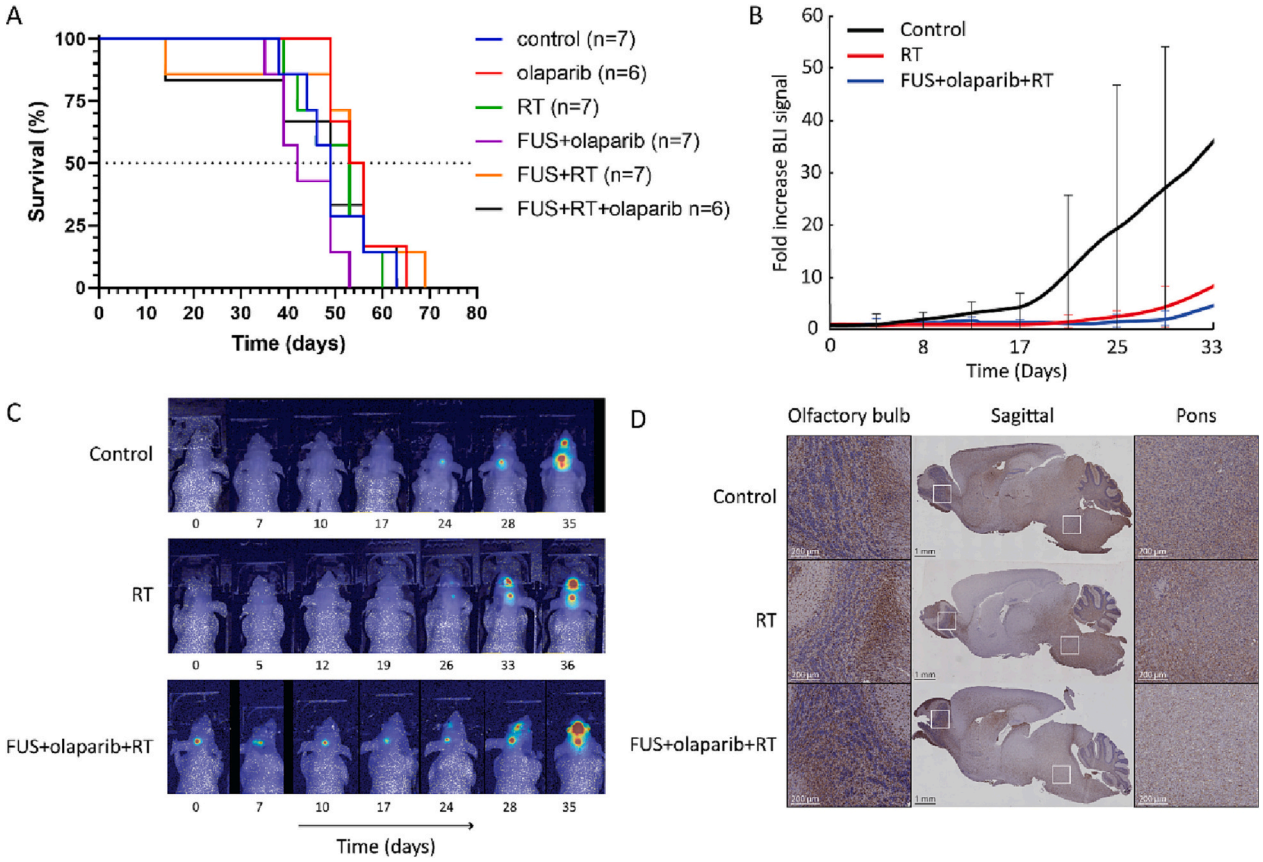

Fig. 6. Survival and tumour growth efficacy upon FUS-BBBO, olaparib and RT. (A) Kaplan-Meier curve showing overall survival following therapy. No significant difference between groups was observed. (B) Tumour growth suppression was observed between control, RT only, and full combination (FUS-BBBO/olaparib/RT) groups at 33 days post treatment in the pons. (C) BLI monitoring of tumour development revealed disease dissemination in control, radiated, and olaparib treated animals. (D) Human vimentin positive cells within the pons and olfactory bulbs of animals showing extensive tumour progression. Fully treated mice (FUS-BBBO/olaparib/RT) had a lower tumour burden within the pons compared to all other groups.

radiosensitisation. To assess tolerability, we used *in vivo* pK profiling to establish the bioavailability of olaparib in healthy brain parenchyma with and without enhanced delivery *via* FUS-BBBO. Our data indicates that 100 mg/kg of olaparib is well tolerated in mice, and that FUS-BBBO promotes an influx of olaparib in the brain without deleterious side effects, as similarly reported [33,49]. Several research groups have previously shown that increased local bioavailability of drugs in the parenchyma can be achieved through FUS-BBBO [35,36,59,60]. In our study, local FUS-enhanced extravasation accomplished a 5.36-fold increase of olaparib in the pons, based on the blood/tissue ratio. In recent years, besides olaparib, multiple PARP inhibitors have been developed of which several have been approved for clinical use [57,61]. Compared to olaparib, niraparib and pamiparib have improved BBB penetration properties, while talazoparib has a better binding efficacy [62–64]. However, due to the lack of good comparative studies, it is unknown to what extent the effectiveness of each PARP inhibitor is. The advantage of FUS-BBBO is local drug delivery, while a BBB permeable drug extravasates into the whole brain, thus losing its regional specificity and potentially increasing neurotoxicity.

In vivo bioavailability results were translated for *in vitro* testing, where we found that inhibition of PAR-synthesis by olaparib in combination with RT lead to acute radiosensitisation as well as delayed proliferation post treatment, observed by limited neurosphere re-growth. Although the degree of PAR-synthesis inhibition can depend on the cell line, this effect was also observed with olaparib doses well below IC_{50} values in both DMG cell lines. From a therapeutic perspective, these results suggest that this treatment strategy could lead to both a reduction in required RT dose, as well as delay of tumour growth progression post therapy. The observation that neurosphere growth delay was similar after both 2 h and 72 h incubations with olaparib in the HSJD-DIPG-007 cell line could suggest that there is a therapeutic window of opportunity within the short period in which FUS-BBBO can be exploited to deliver drugs to the brain parenchyma.

To qualitatively validate if this observation could be exploited *in vivo*, we assessed this treatment combination in a PDX animal model. RT was applied 30 min after olaparib administration, which corresponds to the Tmax and Cmax observed upon pK profiling. Although no survival benefit was observed following treatment, several insights into the potential of this treatment strategy were gained. In both groups where RT alone was applied, a significant reduction in local tumour growth was seen, confirming our *in vitro* observations. When RT was combined with FUS-BBBO and olaparib, a further reduction in local tumour growth, albeit non-significant, confirmed that the radiosensitisation effect we saw *in vitro* was reproducible *in vivo*. This shows that the approach of utilising FUS-BBBO to deliver drugs over a short period of time is feasible. Subsequently, multiple potential radiosensitizers proven to be effective *in vitro* for the treatment of DMG are now also eligible for *in vivo* testing.

Although some positive observations were made, several factors contributed to the lack of therapeutic efficacy in the study. For example, in the PDX model used, rapid disease progression was observed across all groups, with most animals surviving only 40 days post treatment due to severe weight loss, possibly arising from diminished appetite. Indeed, by 33 days post-treatment, widespread disease was observed throughout the brain, including formation of secondary foci. We found severe metastases formations in the olfactory bulbs of the animals, which could

explain the equal survival times across all groups, despite substantially different overall local tumour burden, as a factor of anosmia induced fasting [65]. Olaparib has also been reported to suppress appetite [44], which could additionally contribute to reduced food intake in mice with anosmia. Treatment of animals was initiated 21 days post inoculation of tumour cells, which could be too late for a local therapeutic intervention such as FUS-BBBO to have an effect, due to the presence of locally invasive and metastatic disease [66]. Further studies to assess optimal treatment initiation time, with consideration of treating metastatic areas such as the olfactory bulbs using FUS-BBBO, as well as technical factors such as feasibility in continued FUS-BBBO application, need to be conducted to optimise therapeutic applications of FUS-BBBO in animal models of DMG.

In conclusion, this study has shown that PARP1 inhibition is a promising radiosensitisation strategy for DMG. FUS-BBBO could temporarily enhance olaparib delivery into the brain at clinically relevant values, supported by *in vitro* growth inhibition of DMG cells exposed to olaparib and radiation. Further preclinical studies are needed to determine optimal start of treatment and dosing regimen, as well as timing of FUS-BBBO with improved survival benefit.

Supplementary data to this article can be found online at https://doi.org/10.1016/j.jconrel.2023.03.058.

CRediT authorship contribution statement

E. 't Hart: Validation, Formal analysis, Investigation, Resources, Data curation, Writing – original draft, Visualization. **J. Bianco:** Writing – review & editing, Visualization, Project administration. **M.A.C. Bruin:** Validation, Investigation. **M. Derieppe:** Validation, Investigation, Writing – review & editing, Project administration. **H.C. Besse:** Methodology, Investigation. **K. Berkhout:** Validation, Investigation. **L.A. Chin Joe Kie:** Validation, Investigation. **Y. Su:** Methodology, Resources. **E.W. Hoving:** Writing – review & editing, Supervision. **A.D.R. Huitema:** Writing – review & editing, Supervision. **M.G. Ries:** Conceptualization, Software, Writing – review & editing, Supervision. **D.G. van Vuurden:** Conceptualization, Writing – review & editing, Supervision, Funding acquisition.

Data availability

Data will be made available on request.

Acknowledgements

This project was supported by KWF Young Investigator Award (KWF 10911, Dr. D.G. van Vuurden). The authors thank Dr. Angel Montero Carcaboso (Sant Joan de Déu Barcelona Hospital, Barcelona, Spain) for kindly providing the patient derived DMG cell lines. We also thank Dr. Wissam Beaino for hosting the experiments at the Radionuclide Center (Department of Radiology and Nuclear Medicine, Amsterdam University Medical Center, Amsterdam, Netherlands), Luc Lucas for his technical expertise in LC-MS/MS (Bioanalytical Laboratory of the Pharmacy, Netherlands Cancer Institute, Amsterdam, Netherlands) and Prof. Jan Molenaar for providing plasmids (Princes Máxima Center for Pediatric Oncology, Utrecht, Netherlands). Graphical abstract and Fig. 1 created with BioRender.com

References

[1] D.N. Louis, A. Perry, G. Reifenberger, A. von Deimling, D. Figarella-Branger, W. K. Cavenee, H. Ohgaki, O.D. Wiestler, P. Kleihues, D.W. Ellison, The 2016 World Health Organization classification of tumors of the central nervous system: a summary, Acta Neuropathol. 131 (2016) 803–820, https://doi.org/10.1007/s00401-016-1545-1.

[2] D. Hargrave, U. Bartels, E. Bouffet, Diffuse brainstem glioma in children: critical review of clinical trials, Lancet Oncol. 7 (2006) 241–248, https://doi.org/10.1016/S1470-2045(06)70615-5.

[3] L.M. Hoffman, S.E.M. Veldhuijzen van Zanten, N. Colditz, J. Baugh, B. Chaney, M. Hoffmann, A. Lane, C. Fuller, L. Miles, C. Hawkins, U. Bartels, E. Bouffet, S. Goldman, S. Leary, N.K. Foreman, R. Packer, K.E. Warren, A. Broniscer, M. W. Kieran, J. Minturn, M. Comito, E. Broxson, C.-S. Shih, S. Khatua, M. Chintagumpala, A.S. Carret, N.Y. Escorza, T. Hassall, D.S. Ziegler, N. Gottardo, H. Dholaria, R. Doughman, M. Benesch, R. Drissi, J. Nazarian, N. Jabado, N. Boddaert, P. Varlet, G. Giraud, D. Castel, S. Puget, C. Jones, E. Hulleman, P. Modena, M. Giagnacovo, M. Antonelli, T. Pietsch, G.H. Gielen, D.T.W. Jones, D. Sturm, S.M. Pfister, N.U. Gerber, M.A. Grotzer, E. Pfaff, A.O. von Bueren, D. Hargrave, G.A. Solanki, F. Jadrijevic Cvrlje, G.J.L. Kaspers, W.P. Vandertop, J. Grill, S. Bailey, V. Biassoni, M. Massimino, R. Calmon, E. Sanchez, B. Bison, M. Warmuth-Metz, J. Leach, B. Jones, D.G. van Vuurden, C.M. Kramm, M. Fouladi, Clinical, radiologic, pathologic, and molecular characteristics of long-term survivors of diffuse intrinsic pontine glioma (DIPG): a collaborative report from the international and European society for pediatric oncology DIPG registries, J. Clin. Oncol. 36 (2018) 1963–1972, https://doi.org/10.1200/JCO.2017.75.9308.

[4] M.H. Jansen, S.E. Veldhuijzen van Zanten, E. Sanchez Aliaga, M.W. Heymans, M. Warmuth-Metz, D. Hargrave, E.J. van der Hoeven, C.E. Gidding, E.S. de Bont, O. S. Eshghi, R. Reddingius, C.M. Peeters, A.Y.N. Schouten-van Meeteren, R.H. J. Gooskens, B. Granzen, G.M. Paardekooper, G.O. Janssens, D.P. Noske, F. Barkhof, C.M. Kramm, W.P. Vandertop, G.J. Kaspers, D.G. van Vuurden, Survival prediction model of children with diffuse intrinsic pontine glioma based on clinical and radiological criteria. Neuro Oncol. 17 (2015) 160–166, https://doi.org/10.1093/neuonc/nou104.

[5] R. Stupp, M.E. Hegi, W.P. Mason, M.J. van den Bent, M.J.B. Taphoorn, R.C. Janzer, S.K. Ludwin, A. Allgeier, B. Fisher, K. Belanger, P. Hau, A.A. Brandes, J. Gijtenbeek, C. Marosi, C.J. Vecht, K. Mokhtari, P. Wesseling, S. Villa, E. Eisenhauer, T. Gorlia, M. Weller, D. Lacombe, J.G. Cairncross, R.-O. Mirimanoff, Effects of radiotherapy with concomitant and adjuvant temozolomide versus radiotherapy alone on survival in glioblastoma in a randomised phase III study: 5-year analysis of the EORTC-NCIC trial, Lancet. Oncol. 10 (2009) 459–466, https://doi.org/10.1016/S1470-2045(09)70025-7.

[6] L.P. Lassman, V.E. Arjona, Pontine gliomas of childhood, Lancet. 289 (1967) 913–915, https://doi.org/10.1016/S0140-6736(67)91485-7.

[7] M.S. Ataç, G. Blaauw, Radiotherapy in brain-stem gliomas in children, Clin. Neurol. Neurosurg. 81 (1979) 281-IN11, https://doi.org/10.1016/0303-8467(79)90032-5.

[8] K.E. Warren, Beyond the blood:brain barrier: the importance of central nervous system (CNS) pharmacokinetics for the treatment of CNS tumors, including diffuse intrinsic pontine glioma, Front. Oncol. 8 (2018) 239, https://doi.org/10.3389/fonc.2018.00239.

[9] A. Mackay, A. Burford, D. Carvalho, E. Izquierdo, J. Fazal-Salom, K.R. Taylor, L. Bjerke, M. Clarke, M. Vinci, M. Nandhabalan, S. Temelso, S. Popov, V. Molinari, P. Raman, A.J. Waanders, H.J. Han, S. Gupta, L. Marshall, S. Zacharoulis, S. Vaidya, H.C. Mandeville, L.R. Bridges, A.J. Martin, S. Al-Sarraj, C. Chandler, H.-K. Ng, X. Li, K. Mu, S. Trabelsi, D.H.-B. Brahim, A.N. Kisljakov, D.M. Konovalov, A. S. Moore, A.M. Carcaboso, M. Sunol, C. de Torres, O. Cruz, J. Mora, L.I. Shats, J. N. Stavale, L.T. Bidinotto, R.M. Reis, N. Entz-Werle, M. Farrell, J. Cryan, D. Crimmins, J. Caird, J. Pears, M. Monje, M.-A. Debily, D. Castel, J. Grill, C. Hawkins, H. Nikbakht, N. Jabado, S.J. Baker, S.M. Pfister, D.T.W. Jones, M. Fouladi, A.O. von Bueren, M. Baudis, A. Resnick, C. Jones, Integrated molecular meta-analysis of 1,000 pediatric high-grade and diffuse intrinsic pontine glioma, Cancer Cell 32 (2017) 520–537.e5, https://doi.org/10.1016/j.ccell.2017.08.017.

[10] H. Pedersen, K. Schmiegelow, P. Hamerlik, Radio-resistance and DNA repair in pediatric diffuse midline gliomas, Cancers (Basel). 12 (2020) 2813, https://doi.org/10.3390/cancers12102813.

[11] A. Ashworth, A synthetic lethal therapeutic approach: poly(ADP) ribose polymerase inhibitors for the treatment of cancers deficient in DNA double-strand break repair, J. Clin. Oncol. 26 (2008) 3785–3790, https://doi.org/10.1200/JCO.2008.16.0812.

[12] M. Zarghooni, U. Bartels, E. Lee, P. Buczkowicz, A. Morrison, A. Huang, E. Bouffet, C. Hawkins, Whole-genome profiling of pediatric diffuse intrinsic pontine gliomas highlights platelet-derived growth factor receptor alpha and poly (ADP-ribose) polymerase as potential therapeutic targets, J. Clin. Oncol. 28 (2010) 1337–1344, https://doi.org/10.1200/JCO.2009.25.5463.

[13] Q.T. Ostrom, H. Gittleman, J. Fulop, M. Liu, R. Blanda, C. Kromer, Y. Wolinsky, C. Kruchko, J.S. Barnholtz-Sloan, CBTRUS statistical report: primary brain and central nervous system tumors diagnosed in the United States in 2008–2012, Neuro-Oncology 17 Suppl 4 (2015) iv1–iv62, https://doi.org/10.1093/neuonc/nov189.

[14] A.R. Chaudhuri, A. Nussenzweig, The multifaceted roles of PARP1 in DNA repair and chromatin remodelling, Nat. Rev. Mol. Cell Biol. 18 (2017) 610–621, https://doi.org/10.1038/nrm.2017.53.

[15] D.G. van Vuurden, E. Hulleman, O.L.M. Meijer, L.E. Wedekind, M. Kool, H. Witt, P. W. Vandertop, T. Würdinger, D.P. Noske, G.J.L. Kaspers, J. Cloos, PARP inhibition sensitizes childhood high grade glioma, medulloblastoma and ependymoma to radiation, Oncotarget. 2 (2011) 984–996, https://doi.org/10.18632/oncotarget.362.

[16] Y. Chornenkyy, S. Agnihotri, M. Yu, P. Buczkowicz, P. Rakopoulos, B. Golbourn, L. Garzia, R. Siddaway, S. Leung, J.T. Rutka, M.D. Taylor, P.B. Dirks, C. Hawkins, Poly-ADP-ribose polymerase as a therapeutic target in pediatric diffuse intrinsic pontine glioma and pediatric high-grade astrocytoma, Mol. Cancer Ther. 14 (2015) 2560–2568, https://doi.org/10.1158/1535-7163.MCT-15-0282.

[17] J.M. Senra, B.A. Telfer, K.E. Cherry, C.M. McCrudden, D.G. Hirst, M.J. O'Connor, S. R. Wedge, I.J. Stratford, Inhibition of PARP-1 by olaparib (AZD2281) increases the radiosensitivity of a lung tumor xenograft, Mol. Cancer Ther. 10 (2011) 1949–1958, https://doi.org/10.1158/1535-7163.MCT-11-0278.

[18] S.A. Jannetti, G. Carlucci, B. Carney, S. Kossatz, L. Shenker, L.M. Carter, B. Salinas, C. Brand, A. Sadique, P.L. Donabedian, K.M. Cunanan, M. Gönen, V. Ponomarev, B. M. Zeglis, M.M. Souweidane, J.S. Lewis, W.A. Weber, J.L. Humm, T. Reiner, PARP-1-targeted radiotherapy in mouse models of glioblastoma, J. Nucl. Med. 59 (2018) 1225–1233, https://doi.org/10.2967/jnumed.117.205054.

[19] W. Waissi, A. Nicol, M. Jung, M. Rousseau, D. Jarnet, G. Noel, H. Burckel, Radiosensitizing pancreatic cancer with PARP inhibitor and gemcitabine: an in vivo and a whole-transcriptome analysis after proton or photon irradiation, Cancers (Basel). 13 (2021), https://doi.org/10.3390/cancers13030527.

[20] A.R. Michmerhuizen, A.M. Pesch, L. Moubadder, B.C. Chandler, K. Wilder-Romans, M. Cameron, E. Olsen, D.G. Thomas, A. Zhang, N. Hirsh, C.L. Ritter, M. Liu, S. Nyati, L.J. Pierce, R. Jagsi, C. Speers, PARP1 inhibition radiosensitizes models of inflammatory breast cancer to ionizing radiation, Mol. Cancer Ther. 18 (2019) 2063–2073, https://doi.org/10.1158/1535-7163.MCT-19-0520.

[21] M. Robson, S.-A. Im, E. Senkus, B. Xu, S.M. Domchek, N. Masuda, S. Delaloge, W. Li, N. Tung, A. Armstrong, W. Wu, C. Goessl, S. Runswick, P. Conte, Olaparib for metastatic breast cancer in patients with a germline BRCA mutation, N. Engl. J. Med. 377 (2017) 523–533, https://doi.org/10.1056/NEJMoa1706450.

[22] R. de Haan, E. van Werkhoven, M.M. van den Heuvel, H.M.U. Peulen, G.S. Sonke, P. Elkhuizen, M.W.M. van den Brekel, M.E.T. Tesselaar, C. Vens, J.H.M. Schellens, B. van Triest, M. Verheij, Study protocols of three parallel phase 1 trials combining radical radiotherapy with the PARP inhibitor olaparib, BMC Cancer 19 (2019) 901, https://doi.org/10.1186/s12885-019-6121-3.

[23] P. Loap, D. Loirat, F. Berger, F. Ricci, A. Vincent-Salomon, C. Ezzili, V. Mosseri, A. Fourquet, M. Ezzalfani, Y. Kirova, Combination of olaparib and radiation therapy for triple negative breast cancer: preliminary results of the RADIOPARP phase 1 trial, Int. J. Radiat. Oncol. Biol. Phys. 109 (2021) 436–440, https://doi.org/10.1016/j.ijrobp.2020.09.032.

[24] M.P. Mehta, W.J. Curran, D. Wang, F. Wang, L. Kleinberg, A. Brade, N. Mostafa, J. Qian, T. Leahy, B. Desai, Phase I safety and pharmacokinetic (PK) study of veliparib in combination with whole brain radiation therapy (WBRT) in patients (pts) with brain metastases, Int. J. Radiat. Oncol. 84 (2012) S269–S270, https://doi.org/10.1016/j.ijrobp.2012.07.702.

[25] P. Chabot, T.-C. Hsia, J.-S. Ryu, V. Gorbunova, C. Belda-Iniesta, D. Ball, E. Kio, M. Mehta, K. Papp, Q. Qin, J. Qian, K.D. Holen, V. Giranda, J.H. Suh, Veliparib in combination with whole-brain radiation therapy for patients with brain metastases from non-small cell lung cancer: results of a randomized, global, placebo-controlled study, J. Neuro-Oncol. 131 (2017) 105–115, https://doi.org/10.1007/s11060-016-2275-x.

[26] P.A. Baxter, J.M. Su, A. Onar-Thomas, C.A. Billups, X.-N. Li, T.Y. Poussaint, E. R. Smith, P. Thompson, A. Adesina, P. Ansell, V. Giranda, A. Paulino, L. Kilburn, I. Quaddoumi, A. Broniscer, S.M. Blaney, I.J. Dunkel, M. Fouladi, A phase I/II study of veliparib (ABT-888) with radiation and temozolomide in newly diagnosed diffuse pontine glioma: a Pediatric Brain Tumor Consortium study, Neuro-Oncology 22 (2020) 875–885, https://doi.org/10.1093/neuonc/noaa016.

[27] H.-W. Sim, K.L. McDonald, Z. Lwin, E.H. Barnes, M. Rosenthal, M.C. Foote, E.-S. Koh, M. Back, H. Wheeler, E.P. Sulman, M.E. Buckland, L. Fisher, R. Leonard, M. Hall, D.M. Ashley, S. Yip, J. Simes, M. Khasraw, A randomized phase II trial of veliparib, radiotherapy, and temozolomide in patients with unmethylated MGMT glioblastoma: the VERTU study, Neuro-Oncology 23 (2021) 1736–1749, https://doi.org/10.1093/neuonc/noab111.

[28] I. Sá-Pereira, D. Brites, M.A. Brito, Neurovascular unit: a focus on pericytes, Mol. Neurobiol. 45 (2012) 327–347, https://doi.org/10.1007/s12035-012-8244-2.

[29] B.T. Hawkins, T.P. Davis, The blood-brain barrier/neurovascular unit in health and disease, Pharmacol. Rev. 57 (2005) 173–185, https://doi.org/10.1124/pr.57.2.4.

[30] W.M. Pardridge, Blood-brain barrier delivery, Drug Discov. Today 12 (2007) 54–61, https://doi.org/10.1016/j.drudis.2006.10.013.

[31] A. Burgess, K. Shah, O. Hough, K. Hynynen, Focused ultrasound-mediated drug delivery through the blood-brain barrier, Expert. Rev. Neurother. 15 (2015) 477–491, https://doi.org/10.1586/14737175.2015.1028369.

[32] N. Sheikov, N. McDannold, S. Sharma, K. Hynynen, Effect of focused ultrasound applied with an ultrasound contrast agent on the tight junctional integrity of the brain microvascular endothelium, Ultrasound Med. Biol. 34 (2008) 1093–1104, https://doi.org/10.1016/j.ultrasmedbio.2007.12.015.

[33] N. Sheikov, N. McDannold, F. Jolesz, Y.-Z. Zhang, K. Tam, K. Hynynen, Brain arterioles show more active vesicular transport of blood-borne tracer molecules than capillaries and venules after focused ultrasound-evoked opening of the blood-brain barrier, Ultrasound Med. Biol. 32 (2006) 1399–1409, https://doi.org/10.1016/j.ultrasmedbio.2006.05.015.

[34] H. Cho, H.-Y. Lee, M. Han, J.-R. Choi, S. Ahn, T. Lee, Y. Chang, J. Park, Localized down-regulation of p-glycoprotein by focused ultrasound and microbubbles induced blood-brain barrier disruption in rat brain, Sci. Rep. 6 (2016) 31201, https://doi.org/10.1038/srep31201.

[35] S. Alli, C.A. Figueiredo, B. Golbourn, N. Sabha, M.Y. Wu, A. Bondoc, A. Luck, D. Coluccia, C. Maslink, C. Smith, H. Wurdak, K. Hynynen, M. O'Reilly, J.T. Rutka, Brainstem blood brain barrier disruption using focused ultrasound: a demonstration of feasibility and enhanced doxorubicin delivery, J. Control. Release 281 (2018) 29–41, https://doi.org/10.1016/j.jconrel.2018.05.005.

[36] N. Sheikov, N. McDannold, N. Vykhodtseva, F. Jolesz, K. Hynynen, Cellular mechanisms of the blood-brain barrier opening induced by ultrasound in presence of microbubbles, Ultrasound Med. Biol. 30 (2004) 979–989, https://doi.org/10.1016/j.ultrasmedbio.2004.04.010.

[37] Z.K. Englander, H.-J. Wei, A.N. Pouliopoulos, E. Bendau, P. Upadhyayula, C.-I. Jan, E.F. Spinazzi, N. Yoh, M. Tazhibi, N.M. McQuillan, T.J.C. Wang, J.N. Bruce, P. Canoll, N.A. Feldstein, S. Zacharoulis, E.E. Konofagou, C.-C. Wu, Focused ultrasound mediated blood-brain barrier opening is safe and feasible in a murine pontine glioma model, Sci. Rep. 11 (2021) 6521, https://doi.org/10.1038/s41598-021-85180-y.

[38] N. Todd, Y. Zhang, M. Arcaro, L. Becerra, D. Borsook, M. Livingstone, N. McDannold, Focused ultrasound induced opening of the blood-brain barrier disrupts inter-hemispheric resting state functional connectivity in the rat brain, Neuroimage. 178 (2018) 414–422, https://doi.org/10.1016/j.neuroimage.2018.05.063.

[39] J. Park, Y. Zhang, N. Vykhodtseva, F.A. Jolesz, N.J. McDannold, The kinetics of blood brain barrier permeability and targeted doxorubicin delivery into brain induced by focused ultrasound, J. Control. Release 162 (2012) 134–142, https://doi.org/10.1016/j.jconrel.2012.06.012.

[40] A. Bairoch, The cellosaurus, a cell-line knowledge resource, J. Biomol. Tech. 29 (2018) 25–38, https://doi.org/10.7171/jbt.18-2902-002.

[41] W.M. Kholosy, M. Derieppe, F. van den Ham, K. Ober, Y. Su, L. Custers, L. Schild, L. van Zogchel, L. Wellens, H. Ariese, C.L. Szanto, J. Wienke, M.P. Dierselhuis, D. van Vuurden, E.M. Dolman, J.J. Molenaar, Neuroblastoma and DIPG organoid coculture system for personalized assessment of novel anticancer immunotherapies, J. Pers. Med. 11 (2021) 869, https://doi.org/10.3390/jpm11090869.

[42] C. Kilkenny, W.J. Browne, I.C. Cuthill, M. Emerson, D.G. Altman, Improving bioscience research reporting: the ARRIVE guidelines for reporting animal research, Osteoarthr. Cartil. 20 (2012) 256–260, https://doi.org/10.1016/j.joca.2012.02.010.

[43] L. Qi, M. Kogiso, Y. Du, H. Zhang, F.K. Braun, Y. Huang, W.-Y. Teo, H. Lindsay, S. Zhao, P. Baxter, X. Zhao, L. Yu, Z. Liu, X. Zhang, J.M. Su, A. Adesina, J. Yang, M. Chintagumpala, L. Perlaky, C. Tsz-Kwong Man, C.C. Lau, X.-N. Li, Impact of SCID mouse gender on tumorigenicity, xenograft growth and drug-response in a large panel of orthotopic PDX models of pediatric brain tumors, Cancer Lett. 493 (2020) 197–206, https://doi.org/10.1016/j.canlet.2020.08.035.

[44] Committee for Medicinal Products for Human Use (CHMP), CHMP assessment report Lynparza, London, 2014.

[45] G. Su, L. Qin, X. Su, C. Tao, Y. Wei, Gender-dependent pharmacokinetics of olaparib in rats determined by ultra-high performance liquid chromatography/electrospray ionization tandem mass spectrometry, Biomed. Chromatogr. 34 (2020), e4791, https://doi.org/10.1002/bmc.4791.

[46] R. Spina, D.M. Voss, L. Asnaghi, A. Sloan, E.E. Bar, Flow cytometry-based drug screening system for the identification of small molecules that promote cellular differentiation of glioblastoma stem cells, J. Vis. Exp. (2018), https://doi.org/10.3791/56176.

[47] M. Niepel, M. Hafner, M. Chung, P.K. Sorger, Measuring Cancer drug sensitivity and resistance in cultured cells, Curr. Protoc. Chem. Biol. 9 (2017) 55–74, https://doi.org/10.1002/cpch.21.

[48] N.A.P. Franken, H.M. Rodermond, J. Stap, J. Haveman, C. van Bree, Clonogenic assay of cells in vitro, Nat. Protoc. 1 (2006) 2315–2319, https://doi.org/10.1038/nprot.2006.339.

[49] C.A. Schneider, W.S. Rasband, K.W. Eliceiri, NIH image to ImageJ: 25 years of image analysis, Nat. Methods 9 (2012) 671–675, https://doi.org/10.1038/nmeth.2089.

[50] R. Haumann, E. 't Hart, M.P.P. Derieppe, H.C. Besse, G.J.L. Kaspers, E. Hoving, D. G. van Vuurden, E. Hulleman, M. Ries, A high-throughput image-guided stereotactic neuronavigation and focused ultrasound system for blood-brain barrier opening in rodents, J. Vis. Exp. (2020), https://doi.org/10.3791/61269.

[51] C. Greis, Technology overview: SonoVue (Bracco, Milan), Eur. Radiol. 14 (Suppl. 8) (2004) P11–P15.

[52] M.H.A. Jansen, T. Lagerweij, A.C.P. Sewing, D.J. Vugts, D.G. van Vuurden, C.F. M. Molthoff, V. Caretti, S.J.E. Veringa, N. Petersen, A.M. Carcaboso, D.P. Noske, W. P. Vandertop, P. Wesseling, G.A.M.S. van Dongen, G.J.L. Kaspers, E. Hulleman, Bevacizumab targeting diffuse intrinsic pontine glioma: results of 89Zr-bevacizumab PET imaging in brain tumor models, Mol. Cancer Ther. 15 (2016) 2166–2174, https://doi.org/10.1158/1535-7163.MCT-15-0558.

[53] C.M. Nijenhuis, L. Lucas, H. Rosing, J.H.M. Schellens, J.H. Beijnen, Development and validation of a high-performance liquid chromatography-tandem mass spectrometry assay quantifying olaparib in human plasma, J. Chromatogr. B Anal. Technol. Biomed. Life Sci. 940 (2013) 121–125, https://doi.org/10.1016/j.jchromb.2013.09.020.

[54] European Medicines Agency (EMA), Guideline on bioanalytical method validation. https://www.ema.europa.eu/en/documents/scientific-guideline/guideline-bioanalytical-method-validation_en.pdf n.d.

[55] U.F. and D.A. (FDA), Guidance for industry: bioanalytical method validation guidance for industry bioanalytical method validation. http://www.fda.gov/Drugs/GuidanceComplianceRegulatoryInformation/Guidances/default.htm n.d.

[56] R. Haumann, J.I. Bianco, P.M. Waranecki, P.J. Gaillard, G. Storm, M. Ries, D.G. van Vuurden, G.J.L. Kaspers, E. Hulleman, Imaged-guided focused ultrasound in combination with various formulations of doxorubicin for the treatment of diffuse intrinsic pontine glioma, Transl. Med. Commun. 7 (2022) 8, https://doi.org/10.1186/s41231-022-00115-7.

[57] P. Lesueur, F. Chevalier, J.-B. Austry, W. Waissi, H. Burckel, G. Noël, J.-L. Habrand, Y. Saintigny, F. Joly, Poly-(ADP-ribose)-polymerase inhibitors as radiosensitizers: a systematic review of pre-clinical and clinical human studies, Oncotarget. 8 (2017) 69105–69124, https://doi.org/10.18632/oncotarget.19079.

[58] K. Gandhi, A. Barzegar-Fallah, A. Banstola, S.B. Rizwan, J.N.J. Reynolds, Ultrasound-mediated blood–brain barrier disruption for drug delivery: a systematic review of protocols, efficacy, and safety outcomes from preclinical and clinical studies, Pharmaceutics. 14 (2022) 833, https://doi.org/10.3390/pharmaceutics14040833.

[59] J. Ishida, S. Alli, A. Bondoc, B. Golbourn, N. Sabha, K. Mikloska, S. Krumholtz, D. Srikanthan, N. Fujita, A. Luck, C. Maslink, C. Smith, K. Hynynen, J. Rutka, MRI-guided focused ultrasound enhances drug delivery in experimental diffuse intrinsic pontine glioma, J. Control. Release 330 (2021) 1034–1045, https://doi.org/10.1016/j.jconrel.2020.11.010.

[60] D. Ye, X. Zhang, Y. Yue, R. Raliya, P. Biswas, S. Taylor, Y.-C. Tai, J.B. Rubin, Y. Liu, H. Chen, Focused ultrasound combined with microbubble-mediated intranasal delivery of gold nanoclusters to the brain, J. Control. Release 286 (2018) 145–153, https://doi.org/10.1016/j.jconrel.2018.07.020.

[61] M.C.S. Menezes, F. Raheem, L. Mina, B. Ernst, F. Batalini, PARP inhibitors for breast cancer: germline BRCA1/2 and beyond, Cancers (Basel). 14 (2022), https://doi.org/10.3390/cancers14174332.

[62] K. Sun, K. Mikule, Z. Wang, G. Poon, A. Vaidyanathan, G. Smith, Z.-Y. Zhang, J. Hanke, S. Ramaswamy, J. Wang, A comparative pharmacokinetic study of PARP inhibitors demonstrates favorable properties for niraparib efficacy in preclinical tumor models, Oncotarget. 9 (2018) 37080–37096, https://doi.org/10.18632/oncotarget.26354.

[63] Y. Xiong, Y. Guo, Y. Liu, H. Wang, W. Gong, Y. Liu, X. Wang, Y. Gao, F. Yu, D. Su, F. Wang, Y. Zhu, Y. Zhao, Y. Wu, Z. Qin, X. Sun, B. Ren, B. Jiang, W. Jin, Z. Shen, Z. Tang, X. Song, L. Wang, X. Liu, C. Zhou, B. Jiang, Pamiparib is a potent and selective PARP inhibitor with unique potential for the treatment of brain tumor, Neoplasia. 22 (2020) 431–440, https://doi.org/10.1016/j.neo.2020.06.009.

[64] J. Rudolph, K. Jung, K. Luger, Inhibitors of PARP: number crunching and structure gazing, Proc. Natl. Acad. Sci. 119 (2022), e2121979119, https://doi.org/10.1073/pnas.2121979119.

[65] A.M. Ferris, V.B. Duffy, Effect of olfactory deficits on nutritional status. Does age predict persons at risk? Ann. N. Y. Acad. Sci. 561 (1989) 113–123, https://doi.org/10.1111/j.1749-6632.1989.tb20975.x.

[66] E. 't Hart, J. Bianco, H.C. Besse, L.A. Chin Joe Kie, L. Cornet, K.L. Eikelenboom, T.J. M. van den Broek, M. Derieppe, Y. Su, E.W. Hoving, M.G. Ries, D.G. van Vuurden, Towards standardisation of a diffuse midline glioma patient-derived xenograft mouse model based on suspension matrices for preclinical research, Biomedicines 11 (2023), https://doi.org/10.3390/biomedicines11020527.